Supplement to

Late Cenozoic Sea Surface Temperature evolution of the South Atlantic Ocean

GDGT indices for non-thermal overprints on TEX_{86}

We list the GDGT-based ratios and indices to assess potential non-thermal effects on the GDGT distributions. The numbers correspond to Fig. S1 (panel 2–8) and Fig. S2 (panel 2–8) where the GDGT distributions from Site 696 and U1536, respectively, are displayed.

2. The relative contribution of soil- and marine-derived organic matter in marine sediments can be reconstructed using the branched and isoprenoid tetraether (BIT) index (Hopmans et al., 2004). This index is taken as a proxy for the amount of terrestrial GDGT input, including allochthonous terrestrially-derived isoGDGTs (Weijers et al., 2006) into the marine sediments. BIT index values greater than 0.4, is the threshold above which elevated soil-derived GDGTs are suspected to significantly influence TEX_{86}-derived SST estimates (i.e., >2°C) (Weijers et al., 2006). However, this only applies when brGDGTs are sourced from land, as opposed to marine-sourced (see e.g., discussions in Bijl et al., 2021).

3. The fcren' index evaluates variations in the relative abundance of the crenarchaeol stereoisomer. The index is used to detect 'anomalous' versus 'warm' GDGT distributions, compared to values observed in the modern core-top dataset, which indicates non-thermal contributions, potentially water depth, of the crenarchaeol isomer (O'Brien et al., 2017). The index has a cutoff value at above 0.25.

4. The methane index (MI) detects isoprenoidal GDGT contributions from methanotrophic Euryarchaeota (Zhang et al., 2011). MI values >0.3 conservatively reflect hydrate-impacted sediments and suggest that GDGT distribution might be affected by methanogenic archaea.

5. Anaerobic oxidation of methane (AOM) is characterized by GDGT2/Cren ratio values above 0.2 (Weijers et al., 2011).

6. The GDGT-2/GDGT-3 ratio (Taylor et al., 2013) signals possible overprints by archaeal communities dwelling deeper in the water column. We use a cut-off value of 7. We also survail for abrupt changes in GDGT-2/GDGT-3 ratio as this likely indicate a change in the production depth of the GDGTs, and thus imply a change in build-up of the water column and thus water masses. .(Van Der Weijst et al., 2022)

7. The Methanogenesis index, measured by the GDGT-0/Crenarchaeol ratio (Blaga et al., 2009; Sinninghe Damsté et al., 2009; Taylor et al., 2013) is targeted to detect contributions of isoGDGTs (GDGT-0) from methanogens. Samples with GDGT-0/Crenarchaeol ratio >2 are flagged as outliers for potential contribution by methanogenic archaea.

8. The ΔRing Index (ΔRI) detects deviations from a normal pelagic GDGT composition (Zhang et al., 2016). ΔRI values > 0.3 are thought to represent samples for which GDGT distributions diverge outside that of the modern TEX_{86}-RI relationship, based on the 95% confidence interval of the modern regression.

Site 696 GDGT distributions

The Site 696 GDGT pool consist of 90 ± 5% isoGDGTs and 10 ± 5% brGDGTs, indicating that GDGTs are primarily produced by surface ocean-dwelling Thaumarchaeota., with little influence of soil-derived GDGTs, as indicated by the low BIT index (<0.2) throughout the record (Fig. S1C; panel 2). Additionally, there are no elevated concentrations of specific isoGDGTs pointing to enhanced GDGT contributions by methanotrophic or methanogenic microbes (Fig. S1C; panel 4, 5, 7) (Weijers et al., 2006; Blaga et al., 2009; Zhang et al., 2011), nor non-thermal contributions of the crenarchaeol isomer (Fig. S1C; panel 3) (O'Brien et al., 2017). No samples were identified for the potential influence of deep ocean-dwelling archaea, with GDGT 2/GDGT 3 ratio threshold of above 7 (Fig. S1C; panel 6) (Taylor et al., 2013). In total, 9 samples had higher ΔRI values than the cut off of 0.3 (Fig. S1B, S1C; panel 8) indicating a potential non-thermal overprint on the GDGT distribution and are excluded from SST analysis (Supplementary Table 3).

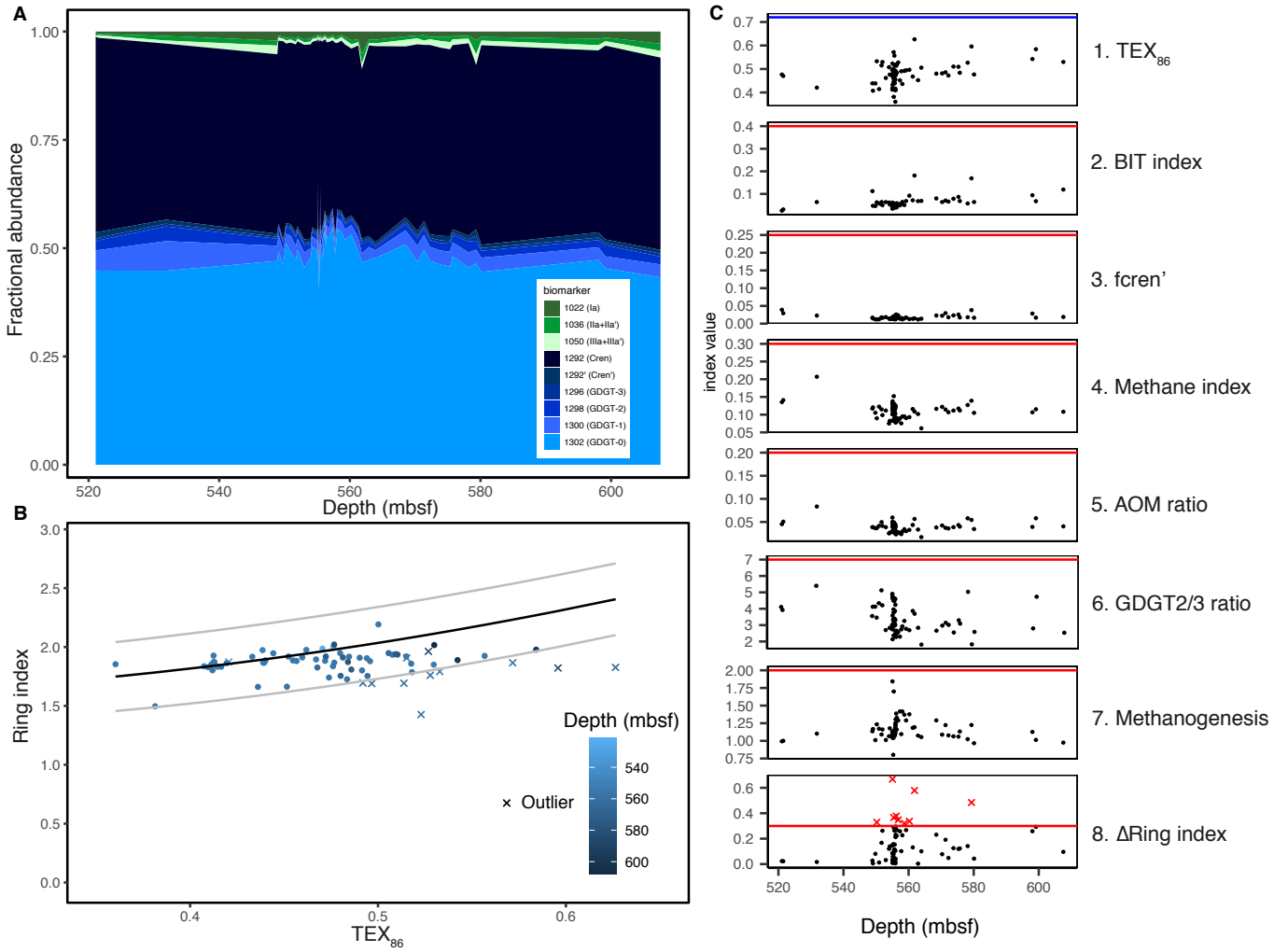

Figure S1. A. ODP Site 696 stacked relative GDGT distribution B. ΔRing Index are plotted relative to TEX_{86} results of Site 696. Black and grey lines represent the RI/TEX_{86} relationship of modern core top samples, and the 95% confidence interval, respectively. Filled circles indicate RI/TEX_{86} values for samples that are retained; crosses indicate samples that are discarded. Color of all data points indicates depth of the sample. C. Site 696 TEX_{86} values and overprinting indices. Red lines indicate the cut-off values used for each of the indices, red crosses indicate samples marked with outlying values to the respective index. 1. TEX_{86} (Schouten et al., 2002), with blue line indicating the maximum modern core-top value (~0.72). 2. BIT index (Hopmans et al., 2004). 3. Fcren' (O'Brien et al., 2017). 4. Methane index (Zhang et al., 2011). 5. AOM ratio (Weijers et al., 2011). 6. GDGT-2/3 ratio (Taylor et al., 2013). 7. Methanogenesis (Blaga et al., 2009), 8. ΔRing index (Zhang et al., 2016).

Site U1536 GDGT distributions

The Site U1536 GDGT pool contain variable amounts of both isoGDGTs and brGDGTs, where brGDGTs are relatively more abundant in the middle (500–560 mbsf) and top parts of the record (440 mbsf) (Fig. S2A). In total, 12 samples had a ΔRI higher than 0.3 (Fig. S2B, C; panel 8) indicating a potential non-thermal overprint on the GDGT distribution. GDGT distributions in 11 of these samples indicate a potential contribution by methanogenic archaea (Methanogenesis index >2), whilst 10 of these same samples also indicate possible soil-derived GDGTs based on high BIT index values (0.4–0.8, Weijers et al., 2006) (Fig. S2C; panel 2). One of the 12 samples discarded for further

analysis had GDGT-2/GDGT-3 ratio value above the threshold of 7 which could indicate a potential influence of deep ocean-dwelling Archaea, (Fig. S2C; panel 7) (Taylor et al., 2013).

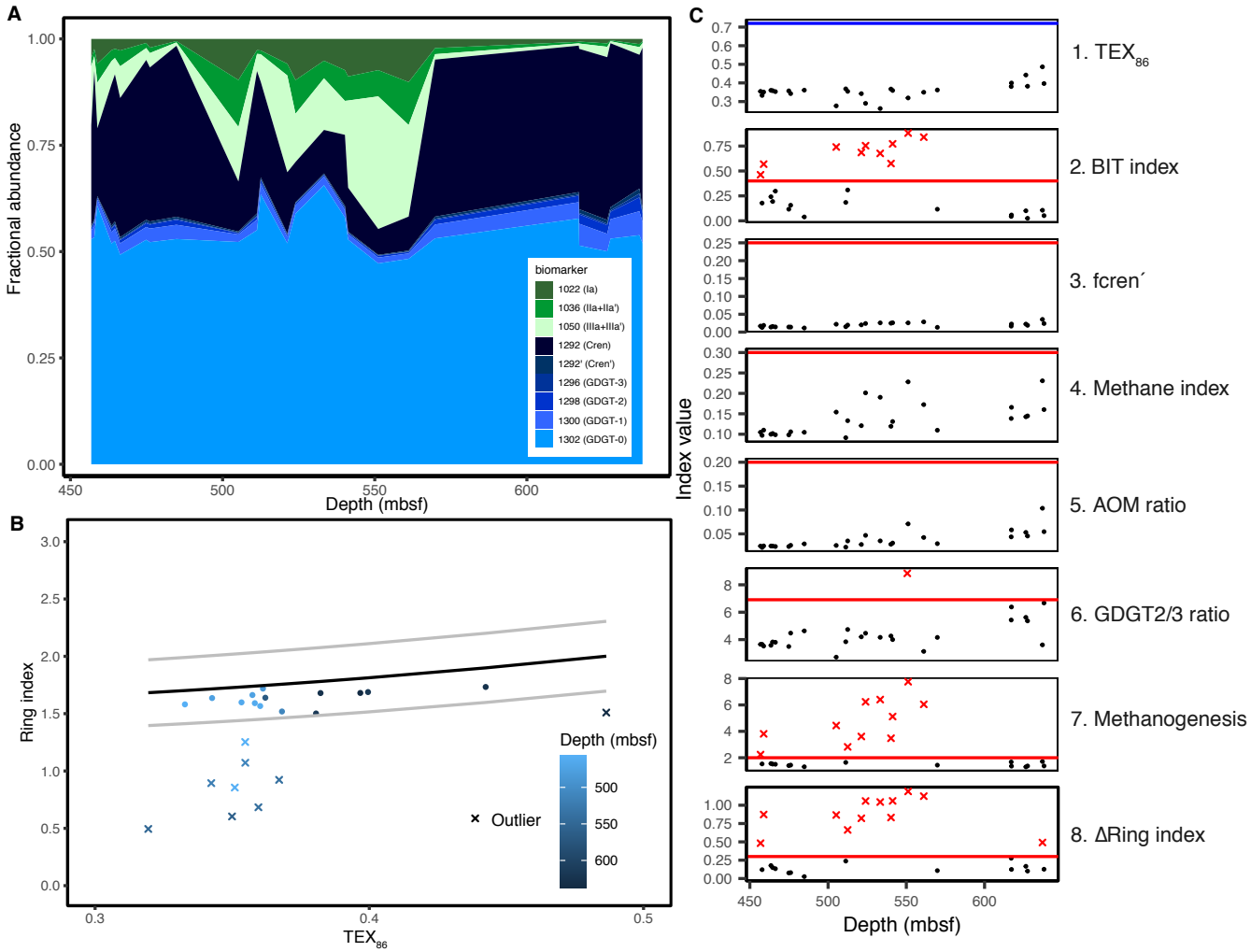

Figure S2. A. IODP Site U1536 stacked relative GDGT distributions. B. ΔRing Index versus TEX_{86}. Black and grey lines represent the RI/TEX_{86} relationship of modern core top samples, and the 95% confidence interval, respectively. Filled circles indicate RI/TEX_{86} values for samples that are retained; crosses indicate samples that are discarded. Color of all data points indicates depth of the sample. C. TEX_{86} values and overprinting indices. Red lines indicate the cut-off values used for each of the indices, red crosses indicate samples marked with outlying values to the respective index. 1. TEX_{86} (Schouten et al., 2002), with blue line indicating the maximum modern core-top value (~0.72). 2. BIT index (Hopmans et al., 2004). 3. Fcren' (O'Brien et al., 2017). 4. Methane index (Zhang et al., 2011). 5. AOM ratio (Weijers et al., 2011). 6. GDGT-2/3 ratio (Taylor et al., 2013). 7. Methanogenesis (Blaga et al., 2009). 8. ΔRing index (Zhang et al., 2016).

Supplementary Table 1: Site 696 age model

Event/Characteristic	Kind	Lower level	Upper level	Bottom depth	Top depth	Mid-depth	Reference	Age (Ma)	Reference biozonation scheme
FAD Denticulopsis maccolummii;	Diatoms	50R-2W, 26-29 cm	50R-1W, 88-92 cm	521.91	521,08	52.49	López-Quirós et al. (in prep.)	16.5-16.7	Harwood and Maruyama (1992); Ramsay and Baldauf (1999); Censarek and Gersonde (2002)

FAAD Actinocyclus ingens	Diatoms	50R-2W, 26-29 cm	50R-1W, 88-92 cm	521.91	521,08	521.49	López-Quirós et al. (in prep.)	16.5-16.7	Harwood and Maruyama (1992); Ramsay and Baldauf (1999); Censarek and Gersonde (2002)
FO Chiropteridium Galea	Dinocysts	53R-3W, 80 cm	53R-2W, 130 cm	552.70	551.70	552.20	*Houben et al. 2012*	<33.6	*Pross et al. (2010)*
FO Malvinia escutiana	Dinocysts	55R-1W, 117 cm	55R-1W, 62 cm	569.39	568.82	569.11	*Houben et al. 2012; 2013*	33.7	*Houben et al. (2011)*
FO Stoveracysta kakanuiensis	Dinocysts	55R-3W, 75 cm	55R-2W, 147 cm	571.95	571.16	571.55	*Houben et al. 2012; 2013*	34.1	*Clowes (1985)*
FO Reticulofenestra oarnaruensis	Calcareous nannofossils	58R-1W, 122 cm	57R-1W, 112 cm	598.42	588.72	588.72	*Wei and Wise, 1990*	~35.5	*Villa et al. (2008)*
FCO Istmolithus recurvus	Calcareous nannofossils	60R-1W, 36 cm	59R-CC	616.96	616.6	616.78	*Wei and Wise, 1990*	36.27	*Villa et al. (2008)*
FO Reticulofenestra bisecta	Calcareous nannofossils	62R-6W, 132 cm	-	643.62	-	643.62	*Wei and Wise, 1990*	<37.61	*Villa et al. (2008)*

Supplementary Table 2: Biostratigraphic datums summarised for the depth of the stratigraphic discontinuities.with sediment reflectors from (Pérez et al., 2021)

Type	Event	Taxa	Published Age (Ma)	Top	Bottom	Mid depth (mbsf)
Hole U1536E						
Reflector-b						
DIAT	LO	*Fragilariopsis praeinterfrigidaria*	3.5	4R-CC	5R-CC	366.37
DIAT	FO	*Rhizosolenia harwoodii*	3.6	4R-CC	5R-CC	366.37
RAD	LO	*Lampromitra coronata*	3.72	4R-CC	5R-CC	366.37
DIAT	LO	*Fragilariopsis aurica*	4.2	7R-CC	9R-CC	403.065
DIAT	LO	*Fragilariopsis praecurta*	4.2	7R-CC	9R-CC	403.065
DIAT	FO	*Fragilariopsis barronii*	4.4	7R-CC	9R-CC	403.065
DIAT	LO	*Denticulopsis delicata*	4.45	7R-CC	9R-CC	403.065
DIAT	LO	*Fragilariopsis arcula*	4.5	7R-CC	9R-CC	403.065
DIAT	LO	*Fragilariopsis curta*	4.7	7R-CC	9R-CC	403.065
RAD	FO	*Helotholus vema*	4.59	7R-CC	9R-CC	403.065
Reflector-c						
PALY	FO	*Operculodinium? eirikianum*	8.4	26R-CC	27R-CC	574.8025
DIAT	FO	*Fragilariopsis aurica*	8.4	30R-CC	31R-CC	613.245
DIAT	FO	*Denticulopsis simonsenii*	14.2	31R-CC	32R-CC	622.58
DIAT	LO	*Denticulopsis maccollumii*	14.3	31R-CC	32R-CC	622.58
PALY	FO	*Impagidinium patulum*	15.97	31R-CC	32R-CC	622.58

Supplementary Table 3: GDGT results Site 696 (attached as separate table)

Supplementary Table 4: GDGT results SiteU1536 (attached as separate table)

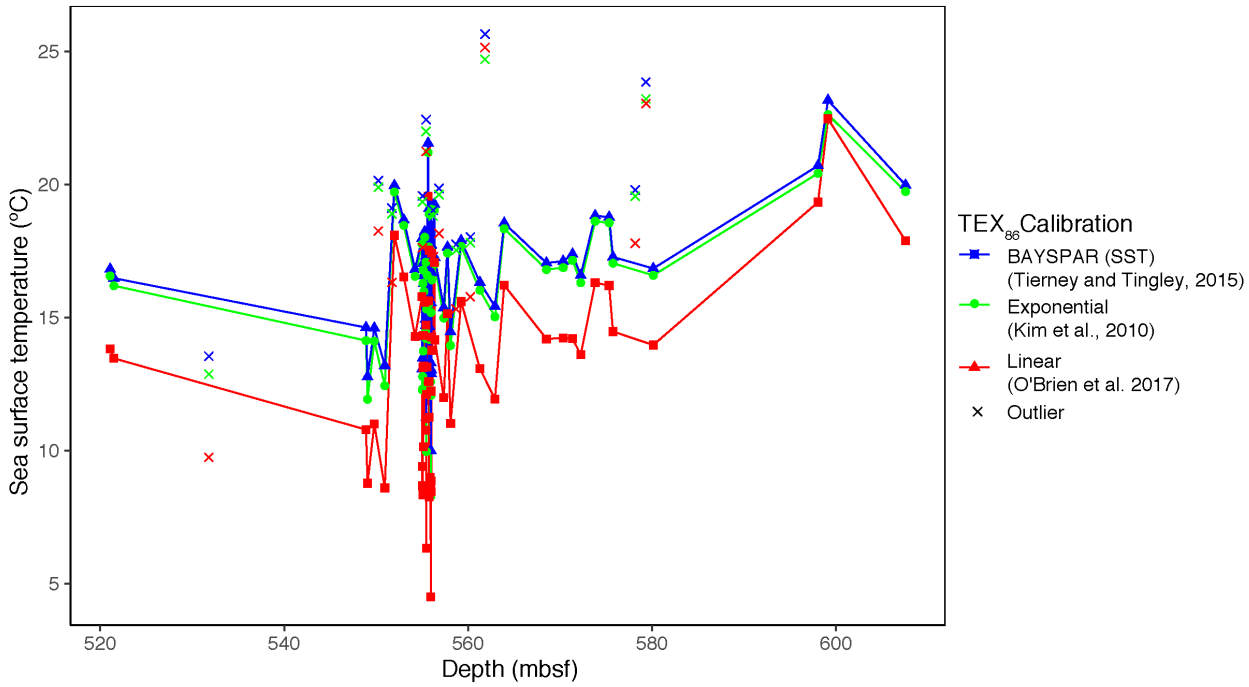

Figure S3. Site 696 TEX_{86} calibration comparison.

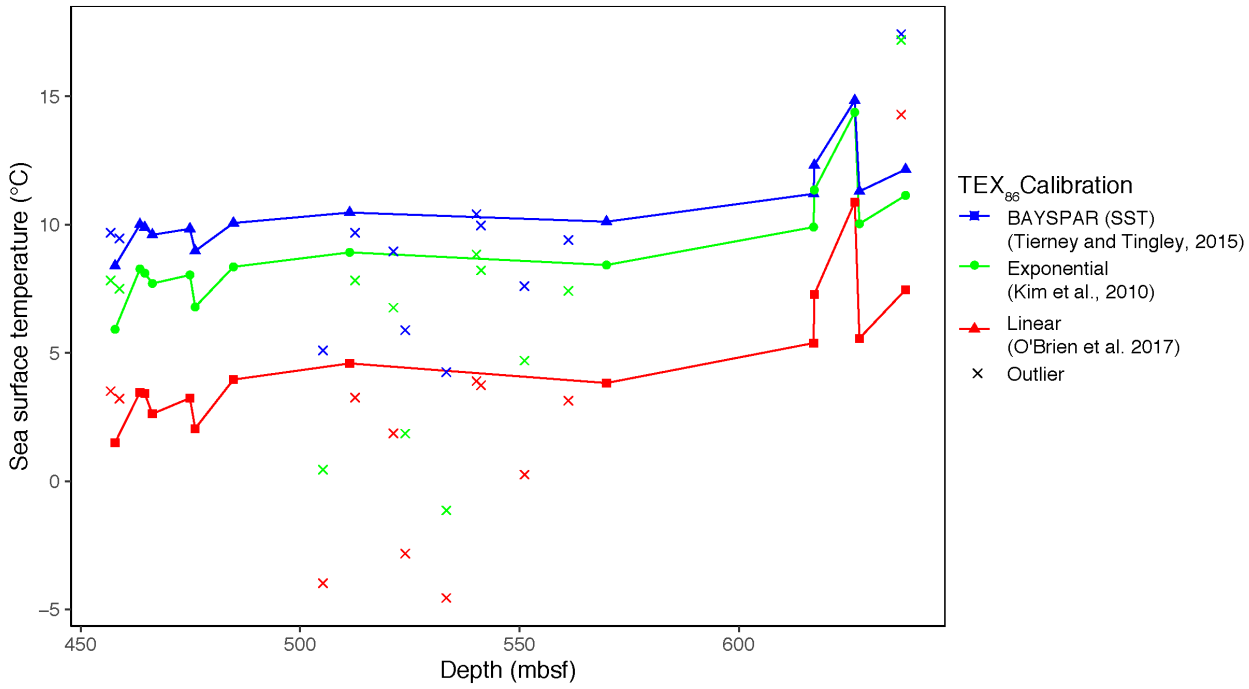

Figure S4. Site U1536 TEX_{86} calibration comparison.

References

Blaga, C. I., Reichart, G.-J., Heiri, O., and Sinninghe Damsté, J. S.: Tetraether membrane lipid distributions in water-column particulate matter and sediments: a study of 47 European lakes along a north–south transect, J Paleolimnol, 41, 523-540, 2009.

Censarek, B., Gersonde, R., 2002. Miocene diatom biostratigraphy at ODP Sites 689, 690, 1088, 1092 (Atlantic sector of the Southern Ocean). Marine Micropaleontology 45, 309–356.

Clowes, C. D.: Stoveracysta, a new gonyaulacacean dinoflagellate genus from the upper Eocene and lower Oligocene of New Zealand, Palynology, 9, 27-35, 1985.

Gersonde, R. and Burckle, L. H.: 43. NEOGENE DIATOM BIOSTRATIGRAPHY OF ODP LEG 113, WEDDELL SEA (ANTARCTIC OCEAN), 1990.

Harwood, D.M., Maruyama, T., 1992. Middle Eocene to Pleistocene diatom biostratigraphy of Southern Ocean sediments from the Kerguelen Plateau, Leg 120. In: Wise Jr. S.W., Schlich, R. et al. (Eds.), Proceedings of the Ocean Drilling Program, Scientific Results, vol. 120(2). Ocean Drilling Program, College Station, TX, pp. 683–733.

Hopmans, E. C., Weijers, J. W., Schefuß, E., Herfort, L., Damsté, J. S. S., and Schouten, S.: A novel proxy for terrestrial organic matter in sediments based on branched and isoprenoid tetraether lipids, Earth and Planetary Science Letters, 224, 107-116, 2004.

Houben, A. J., Bijl, P. K., Guerstein, G. R., Sluijs, A., and Brinkhuis, H.: Malvinia escutiana, a new biostratigraphically important Oligocene dinoflagellate cyst from the Southern Ocean, Rev Palaeobot Palyno, 165, 175-182, 2011.

Houben, A. J., van Mourik, C. A., Montanari, A., Coccioni, R., and Brinkhuis, H.: The Eocene–Oligocene transition: Changes in sea level, temperature or both?, Palaeogeogr Palaeocl, 335, 75-83, 2012.

Houben, A. J., Bijl, P. K., Pross, J., Bohaty, S. M., Passchier, S., Stickley, C. E., Röhl, U., Sugisaki, S., Tauxe, L., and van de Flierdt, T.: Reorganization of Southern Ocean plankton ecosystem at the onset of Antarctic glaciation, Science, 340, 341-344, 2013.

Kim, J.-H., Van der Meer, J., Schouten, S., Helmke, P., Willmott, V., Sangiorgi, F., Koç, N., Hopmans, E. C., and Damsté, J. S. S.: New indices and calibrations derived from the distribution of crenarchaeal isoprenoid tetraether lipids: Implications for past sea surface temperature reconstructions, Geochimica et Cosmochimica Acta, 74, 4639-4654, 10.1016/j.gca.2010.05.027, 2010.

López-Quirós, A., Nieto, F., Garcia-Casco, A., Hoem, F.S., Harwood, D., Morales-Ocaña, C., Bohoyo, F., Escutia, C. Bijl, P.K. Insights into the development of Jane Basin, northern Weddell Sea (Antarctica): Diagenetic constraints on marine sediments from ODP Site 696. In prep.

O'Brien, C. L., Robinson, S. A., Pancost, R. D., Damsté, J. S. S., Schouten, S., Lunt, D. J., Alsenz, H., Bornemann, A., Bottini, C., and Brassell, S. C.: Cretaceous sea-surface temperature evolution: Constraints from TEX86 and planktonic foraminiferal oxygen isotopes, Earth-Sci Rev, 172, 224-247, 2017.

Pérez, L. F., Martos, Y. M., García, M., Weber, M. E., Raymo, M. E., Williams, T., Bohoyo, F., Armbrecht, L., Bailey, I., and Brachfeld, S.: Miocene to present oceanographic variability in the Scotia Sea and Antarctic ice sheets dynamics: Insight from revised seismic-stratigraphy following IODP Expedition 382, Earth and Planetary Science Letters, 553, 116657, 2021.

Ramsay, A.T.S., Baldauf, J.G., A reassessment of the Southern Ocean biochronology, Geological Society Memoir, vol. 18. The Geological Society, London, 1999.

Sinninghe Damsté, J. S., Ossebaar, J., Abbas, B., Schouten, S., and Verschuren, D.: Fluxes and distribution of tetraether lipids in an equatorial African lake: constraints on the application of the TEX86 palaeothermometer and BIT index in lacustrine settings, Geochimica et Cosmochimica Acta, 73, 4232-4249, 2009.

Taylor, K. W., Huber, M., Hollis, C. J., Hernandez-Sanchez, M. T., and Pancost, R. D.: Re-evaluating modern and Palaeogene GDGT distributions: Implications for SST reconstructions, Global Planet Change, 108, 158-174, 10.1016/j.gloplacha.2013.06.011, 2013.

Tierney, J. E. and Tingley, M. P.: A TEX 86 surface sediment database and extended Bayesian calibration, Scientific data, 2, 1-10, 2015.

van der Weijst, C. M., van der Laan, K. J., Peterse, F., Reichart, G.-J., Sangiorgi, F., Schouten, S., Veenstra, T. J., and Sluijs, A.: A 15-million-year surface-and subsurface-integrated TEX 86 temperature record from the eastern equatorial Atlantic, Climate of the Past, 18, 1947-1962, 2022.

Villa, G., Fioroni, C., Pea, L., Bohaty, S., and Persico, D.: Middle Eocene–late Oligocene climate variability: calcareous nannofossil response at Kerguelen Plateau, Site 748, Marine Micropaleontology, 69, 173-192, 2008.

Wei, W. and Wise Jr, S. W.: Biogeographic gradients of middle Eocene-Oligocene calcareous nannoplankton in the South Atlantic Ocean, Palaeogeography, Palaeoclimatology, Palaeoecology, 79, 29-61, 1990.

Weijers, J. W., Schouten, S., Spaargaren, O. C., and Damsté, J. S. S.: Occurrence and distribution of tetraether membrane lipids in soils: Implications for the use of the TEX86 proxy and the BIT index, Organic Geochemistry, 37, 1680-1693, 2006.

Weijers, J. W., Lim, K. L., Aquilina, A., Sinninghe Damsté, J. S., and Pancost, R. D.: Biogeochemical controls on glycerol dialkyl glycerol tetraether lipid distributions in sediments characterized by diffusive methane flux, Geochemistry, Geophysics, Geosystems, 12, 2011.

Zhang, Y. G., Zhang, C. L., Liu, X.-L., Li, L., Hinrichs, K.-U., and Noakes, J. E.: Methane Index: A tetraether archaeal lipid biomarker indicator for detecting the instability of marine gas hydrates, Earth and Planetary Science Letters, 307, 525-534, 10.1016/j.epsl.2011.05.031, 2011.

Zhang, Y. G., Pagani, M., and Wang, Z.: Ring Index: A new strategy to evaluate the integrity of TEX86 paleothermometry, Paleoceanography, 31, 220-232, 10.1002/2015pa002848, 2016.